Structure Development upon Melt Drawing of Ultrahigh Molecular Weight Polyethylene: Effect of Prior Thermal History

Mitsuhiro Nakae, Hiroki Uehara,† and Tetsuo Kanamoto*

Department of Applied Chemistry, Science University of Tokyo, Kagurazaka, Shinjuku-ku, Tokyo 162-8601, Japan

Anagnostis E. Zachariades

POLTECO. Inc., P.O. Box 2055, Burlingame, California 94011-2055

Roger S. Porter

Polymer Science & Engineering Department, University of Massachusetts, Amherst, Massachusetts 01003

Received August 9, 1999; Revised Manuscript Received February 4, 2000

ABSTRACT: The effect of thermal history on the melt drawing of ultrahigh molecular weight polyethylene (UHMWPE) reactor powder was studied. The samples for drawing were prepared by compression-molding of reactor powder at various temperatures above the melting point (T_m). The drawing temperature (T_d) was 150 °C. It was found that the maximum achievable draw ratio at the optimum T_d decreased from 60 to 23 when the prior-melt temperature increased from 160 to 230 °C. The highly drawn films exhibited tensile moduli ≤58 GPa and strength ≤0.95 GPa at room temperature. Scanning electron microscopy (SEM) observations of the drawn films, etched by fuming nitric acid, revealed a characteristic "shish kebab" structure, as reported. Consistent with such morphology, differential scanning calorimetry (DSC) showed double melting endotherms at 134 and 143 °C, corresponding to the "kebob" and "shish" components, respectively. The crystallinity evaluated by the total heat of fusion from the double peaks increased steadily with the draw ratio, and the increase was more rapid for the samples that were prior-melted at a higher temperature and/or for a longer time. The formation of "shish" and "kebob" components and their crystal sizes were also significantly influenced by the prior-melting temperature and the elongation ratio. The efficiency of the draw, evaluated from the fraction of the "shish" component and the tensile properties vs draw ratio, was also interpreted from the differences of the prior-melt preparation conditions. The results suggest that the different level of entanglement formation, which was associated with the scale of segmental diffusion, affected significantly the resultant structure and properties.

Introduction

Ultrahigh molecular weight polyethylene (UHMWPE), in the form of gels[1,2] or single-crystal aggregates,[3,4] has been shown to be ultradrawable in the solid state, producing highly oriented, high modulus and strength fibers and films. The high ductility of the solution-crystallized morphologies has also been reported for other crystalline polymers, including isotactic polypropylene[5,6] and poly(4-methyl-1-pentene),[7] poly(ethylene terephthalate),[8] and poly(acrylonitrile).[9,10] The key to this process is to prepare a less entangled morphology by dissolution of a polymer in a solvent, followed by solidification and removal of the solvent.[11]

It has also been shown that billets and films of UHMWPE reactor powder, compacted below the melting temperature (T_m), could be ultradrawn by solid-state extrusion,[12] coextrusion,[13] and a two-stage draw technique.[14] The latter consists of the initial solid-state coextrusion[15] of a compacted powder film, followed by the second-stage tensile drawing at controlled conditions. Highly drawn products exhibit tensile moduli ≤135 GPa, comparable to those of commercial gel-spun fibers. Independently, Smith et al.[16,17] also have reported ultradrawing of virgin UHMWPE, prepared by using a low-activity catalyst and at low temperatures. For the direct drawing of UHMWPE from reactor powder, ductility increases with powder crystallinity.[18]

Nascent reactor powders of other crystalline polymers, such as poly(tetrafluoroethylene)[19] and poly(acrylonitrile),[20] were also shown to be ultradrawable. However, once the powder was melted, such an excellent ductility was lost in the crystalline state.[19,21] The high ductility of these reactor powders was ascribed also to the low entanglement state of the virgin morphology.[16,17,22,23] One characteristic of the reactor powder draw is the absence of any solvent treatment, which is the key feature in the gel spinning/drawing technique.

The high drawability of UHMWPE reactor powder can be retained even after a prior-melt treatment,[24−27] under controlled melt draw conditions. Upon solid-state drawing, however, the same starting sample exhibited only poor ductility, suggesting major entanglement formation during the prior-melt treatment. The high drawability attained from the melt suggests that the formed entanglements hinder less the high uniaxial elongation, as compared to the deformation in the crystalline state. Further, the stress/strain curves for drawing UHMWPE from melt were markedly affected by the prior-melt treatment temperature and time and the draw rate.[27] This suggests that the entanglement effects change depending on these variables. The slow segmental diffusion in the highly viscous melt of UH-

* To whom correspondence should be addressed.
† Present address: Department of Chemistry, Gunma University, Kiryu, Gunma 376-8515, Japan.

10.1021/ma991330a CCC: $19.00
Published on Web 03/17/2000

MWPE, associated with the melting conditions, likely leads to the formation of apparently different types of molecular entanglements, "shallow" and "deep",[27] depending on the draw rate. The entanglements, which were associated with large-scale segmental diffusion at higher melt temperatures or at longer times, are defined as "deep". They effectively transmit the tensile stress on draw within the melt. The "shallow" entanglements are associated with short-range segmental diffusion at lower temperatures for shorter times. These entanglements can be readily disentangled during melt drawing.[27] Such different characteristics and responses of molecular entanglements may affect the development of oriented morphology and the resultant properties of drawn products.

The purposes of this study are to examine the effect of prior-melt conditions on the structural development in UHMWPE reactor powder during drawing from melt and to evaluate the resultant tensile properties of drawn products.

Experimental Section

Sample Preparation. The UHMWPE reactor powder used was Hizex Million 340M, supplied by Mitsui Chemicals Co. Ltd. It had a viscosity-average molecular weight of 3.3×10^6. Melt-grown crystal (MGC) films 0.2 mm thick were prepared by compression-molding of the reactor powder, which contained a small amount of an antioxidant 3-(3,5-di-*tert*-butyl-4-hydroxy)phenyl propanate (0.5 wt %, based on polymer) at a press temperature (T_p) of 160−230 °C and 2.5 MPa for 5 min, followed by slow cooling to room temperature. A few MGC samples were also prepared by compression-molding after melt annealing at 200 °C for 5−120 min in order to evaluate the effect of prior-melt annealing time (t_a) on the structure formation upon drawing.

Drawing. The films of various thermal histories were cut into strips of 30−70 × 2 × 0.2 mm. These strips were drawn by a tensile force at an established optimum temperature of 150 °C, about 15 °C above their melting temperatures, at a constant cross-head speed corresponding to an initial strain rate of 5/min in an air oven equipped with a Tensilon HTM-100 tensile tester. The draw was initiated after keeping the sample at the draw temperature (T_d) for 5 min to achieve the temperature equilibrium. The draw ratio (DR) was determined from the separation of ink marks preprinted on the sample surface.

Etching Treatment by Fuming Nitric Acid. To emphasize the crystalline morphology of melt-drawn samples for SEM observations, the samples were etched with fuming nitric acid. The etching was made at 60 °C for 24−48 h by adding an excess amount of fuming nitric acid (10 mL) to 0.2 g of a drawn sample, contained in a glass sample tube. After the acid treatment for a given period of time, the sample was washed first by distilled water, subsequently by boiling acetone, and then dried well at room temperature.

Measurements. Differential scanning calorimetry (DSC) was made on a Seiko Denshi DSC-10 and -220. The heating scans were made at a rate of 3 °C/min up to 180 °C under a nitrogen gas flow. The sample melting was evaluated by the melting-peak temperature ($T_{m,peak}$). The heats of fusion (ΔH_f) and $T_{m,peak}$ were calibrated by an indium standard. To avoid the melting of a sample under a constrained state and delay in the heat transfer during heating scan, a small amount of silicone oil was placed between the sample and the bottom of a DSC sample pan. It was confirmed that the DSC baseline was stable even with silicone oil. The decomposition of double melting peaks into two peaks was made assuming Extreme 4/Lorentz functions.

The tensile modulus and strength on the fiber axis were measured at room temperature and strain rates of 1×10^{-1} and 1×10^{-2} s^{-1}, respectively. The modulus was determined from the slope of the stress/strain curve at low strain (<0.1%).

Table 1. DR_{max} and the Resultant Crystallinity Calculated from Density for Drawing from the Melts of MGC Films Prepared at Different T_p's for 5 min; Drawing Was Made at T_d = 150 °C and Constant Cross-Head Speeds Corresponding to an Initial Strain Rate of 5 min^{-1}

T_p (°C)	160	180	200	230
DR_{max}	60	52	45	23
density (g/cm^3)	0.952	0.954	0.950	0.951
crystallinity (%)	69	70	68	68

The cross-sectional area of a sample was calculated from the sample weight, length, and measured density. The densities of the samples were determined at 30 °C in a density gradient column consisting of mixtures of methylcarbitol and 2-propanol.

The crystallinities of samples were determined from their densities and heats of fusion assuming an amorphous/crystalline two-phase model. The crystalline and amorphous densities were taken to be 1.00 and 0.855 g/cm^3, respectively.[28] The heat of fusion for a perfect polyethylene crystal was assumed to be 290 J/g.[28]

Wide-angle (WAXD) and small-angle (SAXS) X-ray scattering patterns were recorded photographically on flat-plate cameras equipped with imaging plates. The sample-to-film distances were 3.5 cm for WAXD and 40 cm for SAXS measurements. Cu Kα radiation monochromatized with a graphite monochromator was generated at 40 kV and 40−150 mA by a Rigaku type RAD-III or a Rigaku type RU-200 rotating-anode X-ray generator.

Scanning electron microscopic (SEM) observations were made on fuming nitric acid-etched samples by a Hitachi S-5000 electron microscope operated at 5 kV. Pt−Pd was evaporated on sample surfaces.

Results and Discussion

The draw behavior of UHMWPE from the melt has been discussed in a previous paper[27] in terms of the observed stress/strain characteristics. The present work focuses on the morphology development during drawing from the melt and the resultant properties of drawn products.

Effect of T_p and t_a on Drawability. The drawability of MGC films from their molten states was found to be significantly affected by several variables, including the draw temperature (T_d) and rate and the prior-melt treatment temperature T_p and time t_a.[27] The optimum T_d resulting in the highest draw was 150 °C, independent of the prior T_p, as reported. Thus, in this work, T_d was fixed at 150 °C, and the draw was carried out at a constant cross-head speed that gave an initial strain rate of 5 min^{-1}, which was optimum for the drawing of the MGC series at T_d = 150 °C. The maximum achievable DR (DR_{max}) for the MGC series decreased with increasing T_p, from 60 at T_p = 160 °C to 23 at T_p = 230 °C, as shown in Table 1. Such changes in DR_{max} with T_p can be interpreted by entanglement differences. It was also shown that the apparent depth of an entanglement depends on both T_d and the draw rate.[27] "Shallow" entanglements formed at *a* lower T_p of 160 °C seem to disentangle easily during draw at T_d = 150 °C, resulting in a higher DR_{max}. In contrast, "deep" entanglements formed at *a* higher T_p of 230 °C effectively transmit the draw stress within the melt but hinder high elongation. The effect of these different entanglement characteristics on the structural development upon drawing at the optimum T_d of 150 °C is discussed below, based on the results obtained for the MGC series prepared at different T_p's for a constant t_a of 5 min. A few data showing the effect of t_a are also reported.

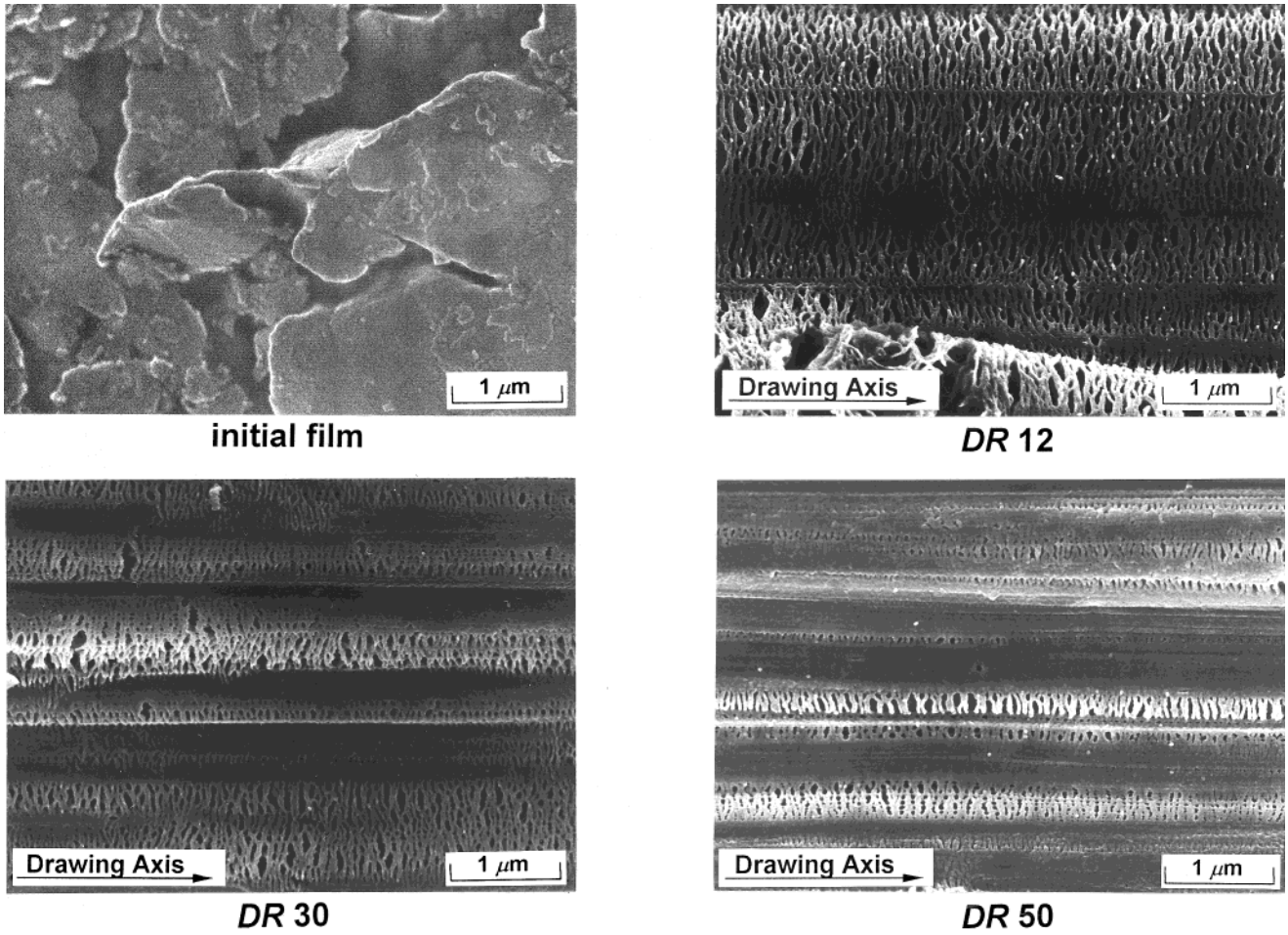

Figure 1. Low-magnification SEM images of an initial MGC film compression-molded at T_p = 180 °C for 5 min and its drawn samples prepared at T_d = 150 °C. The samples were etched by fuming nitric acid at 60 °C for 48 h.

Structure Development during Drawing from Melt. The crystallinities (χ_c) of the products drawn to the DR_{max} were determined from the sample densities and are shown in Table 1 for a series of MGC films prepared at different T_p's. The initial densities of the undrawn films were approximately ~0.936 g/cm^3, corresponding to a χ_c of ~55%. The crystallinity was independent of the prior-melt temperature T_p. The χ_c gradually increased with DR and finally approached the common maximum of ~70% at the DR_{max} for the entire T_p series. As stated, a higher DR_{max} was obtained for drawing a sample of a lower T_p than for one of a higher T_p. These observations indicate that the strain-induced crystallization proceeded more rapidly with DR for the higher T_p films, consistent with the DSC data discussed later. The maximum crystallinity of ~70% achieved for drawing from the melt was significantly higher than those (52−55%) of the initial MGC samples. Nevertheless, the χ_c value was markedly lower than that (~95%) reported for superdrawing of a less entangled single-crystal mat in the solid state.[4] This indicates that although the entanglements formed at the prior-melt on molding effectively induce the segmental orientation by transmitting the applied stress within a melt, they could not all be disentangled even at higher extension.

SEM Observations. The crystallization behavior during draw from the melt for a series of different T_p films was analyzed by the morphology of the drawn products, as revealed by SEM microscopy. Since the as-drawn products revealed no characteristic surface morphologies, the crystalline structure was emphasized by selectively etching the amorphous regions with fuming nitric acid. Figure 1 shows SEM images for a series of draw ratios, prepared from the MGC film molded at T_p = 180 °C. Figure 2 shows high-magnification images of the samples in Figure 1. For the initial undrawn film, crystalline domains with a radius of ~1 μm are revealed on the film surface. The domain size corresponds to that of the subparticles in the untreated initial UHMW-PE reactor powder,[29] indicating that the boundary between the initial subparticles remained even after compression-molding above the sample T_m. Such a survival of the initial particle boundary[26,30,31] indicates that memory loss of the initial particle morphology was not achieved by molding of the UHMWPE powder at 180 °C (~40 °C above the T_m) for 5 min due to its high melt viscosity.

Barham and Sadler[32] found in their neutron-scattering studies that when single-crystal mats of polyethylene were molten, the radii of gyration reached equilibrium values in a few seconds for $M_w < 4 \times 10^5$. However, a highly entangled system of ultrahigh molecular weight exhibits behavior markedly different from that of single-crystal aggregates that actually have no entanglements before melting. Indeed, the reputation time in the molten state for an UHMWPE with M_w 4 × 10^6 was estimated to be ~2.3 h.[32] Further, Millaud and Rault[33,34] have shown that when the melt-annealing temperature (corresponding to T_p in this work) of polyethylene is altered, the time τ required for polyethylene coils to reach their equilibrium dimension at the new temperature is given by the law $\tau \sim M^3$. They also found that this time is of the order of several minutes for a

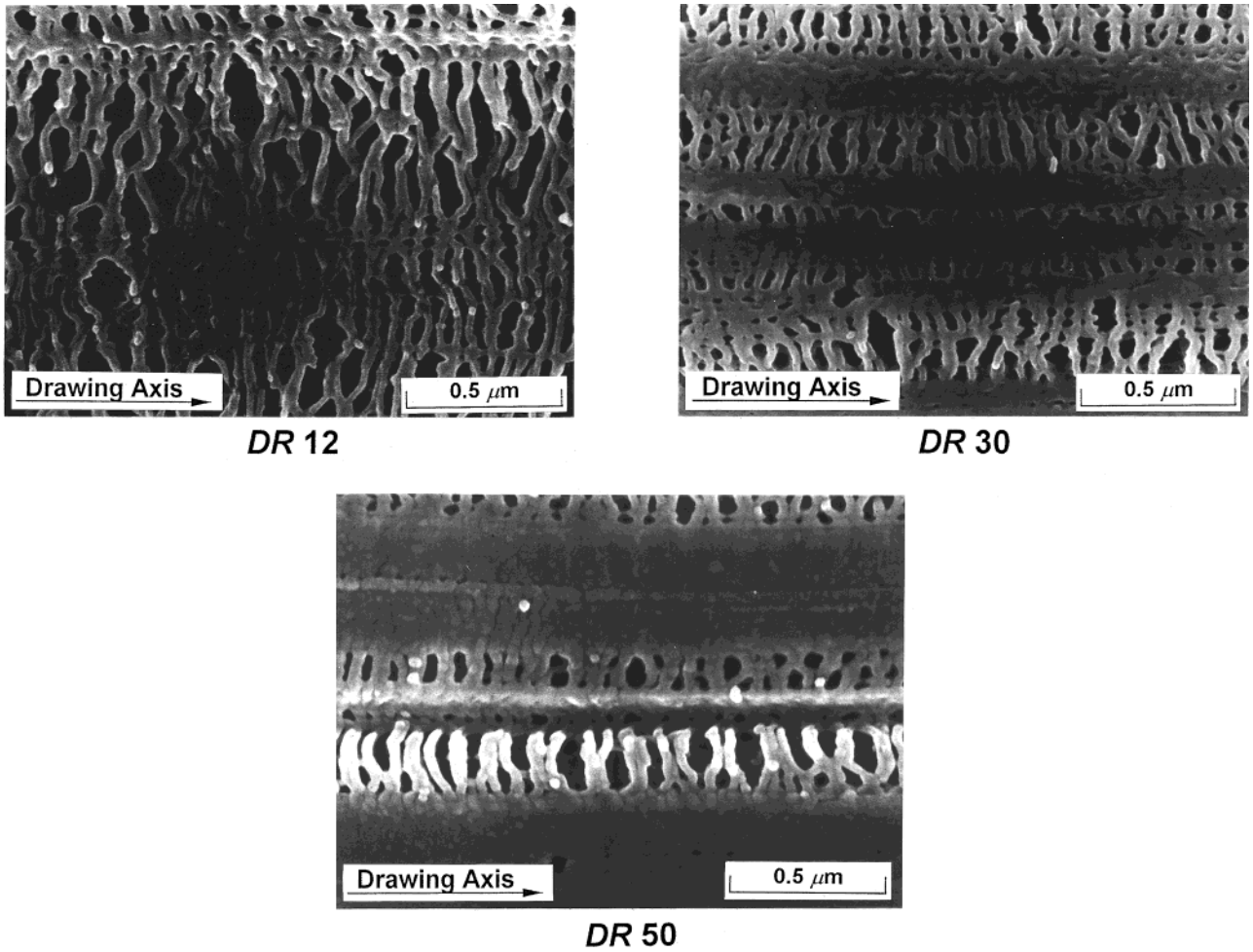

Figure 2. High-magnification SEM images of the samples in Figure 1.

monodisperse sample of $M = 6 \times 10^4$ and 4 h for a polydisperse sample of $M_w = 5 \times 10^5$. Thus, the origin of the high ductility of UHMWPE melts observed in this work may be attributed to this memory retention both at the interface between reactor powders and within a powder even after the melt treatment, due to the slow self-diffusion of UHMWPE and the initially less entangled reactor powder morphology.

The drawn products exhibited a typical "shish kebab" structure, as previously reported.[25,26,35] At a lower DR of 12, a few extended "shish" crystals were observed, and the chain-folded "kebob" crystals, which were epitaxially grown perpendicularly to the draw direction, were the major component. With increasing DR, the lateral size of the "shish" crystals increased as seen in the high-magnification images in Figure 2. At higher DR's of 30 and 50, the "shish" crystals were clearly observed in the SEM images. The thickness of the "kebob" crystals remained 30−50 nm, independent of DR.

The remarkable effect of the prior T_p on the drawn crystalline morphology was observed by SEM. Figure 3 shows sets of low- and high-magnification SEM images for the samples drawn from the MGC film prepared at the highest T_p of 230 °C. When the photographs in Figures 1−3 were compared at a comparable DR, the "shish" content was higher for a higher T_p of 230 °C in Figure 3 than for a lower T_p of 180 °C in Figures 1 and 2. Moreover, the thickness of the "kebob" crystals for the T_p = 230 °C series (50−120 nm in Figure 3) was markedly larger than that for the T_p = 180 °C series (30−50 nm in Figures 1 and 2). Reflecting these crystalline characteristics, the crystallinity for a T_p = 230 °C series increased up to the same level as that of lower T_p series at each DR_{max} (see Table 1), despite its lower DR_{max}.

DSC Melting Behavior. The remarkable effects of the prior T_p and sample DR were also observed on the DSC melting behavior. DSC thermograms for the draw ratio series of MGC films prepared by prior-compression-molding at the lowest T_p of 160 °C and the highest T_p of 230 °C for 5 min are shown in Figures 4 and 5, respectively. Figure 4 shows that at lower DR below ~10 a single melting peak was observed around 134 °C. Upon drawing to a DR of 12, a new endothermic tail appeared at the higher temperature side of the original 134 °C peak. This new endotherm grew steadily with increasing DR and became a major and sharp peak at a DR of 50, near the DR_{max}. In contrast, the initial lower-temperature peak became smaller and broader with increasing DR. The DSC thermograms of the DR series prepared from a film molded at the highest T_p = 230 °C also exhibited similar changes in the characteristics of thermograms with DR as shown in Figure 5. However, when the higher-temperature melting peaks were compared at a DR of 20, the relative peak area was markedly larger for the product from the T_p = 230 °C film than for that from the lower T_p = 160 °C film (Figure 4). The increase of the entropy due to randomization of the oriented amorphous chains, which may

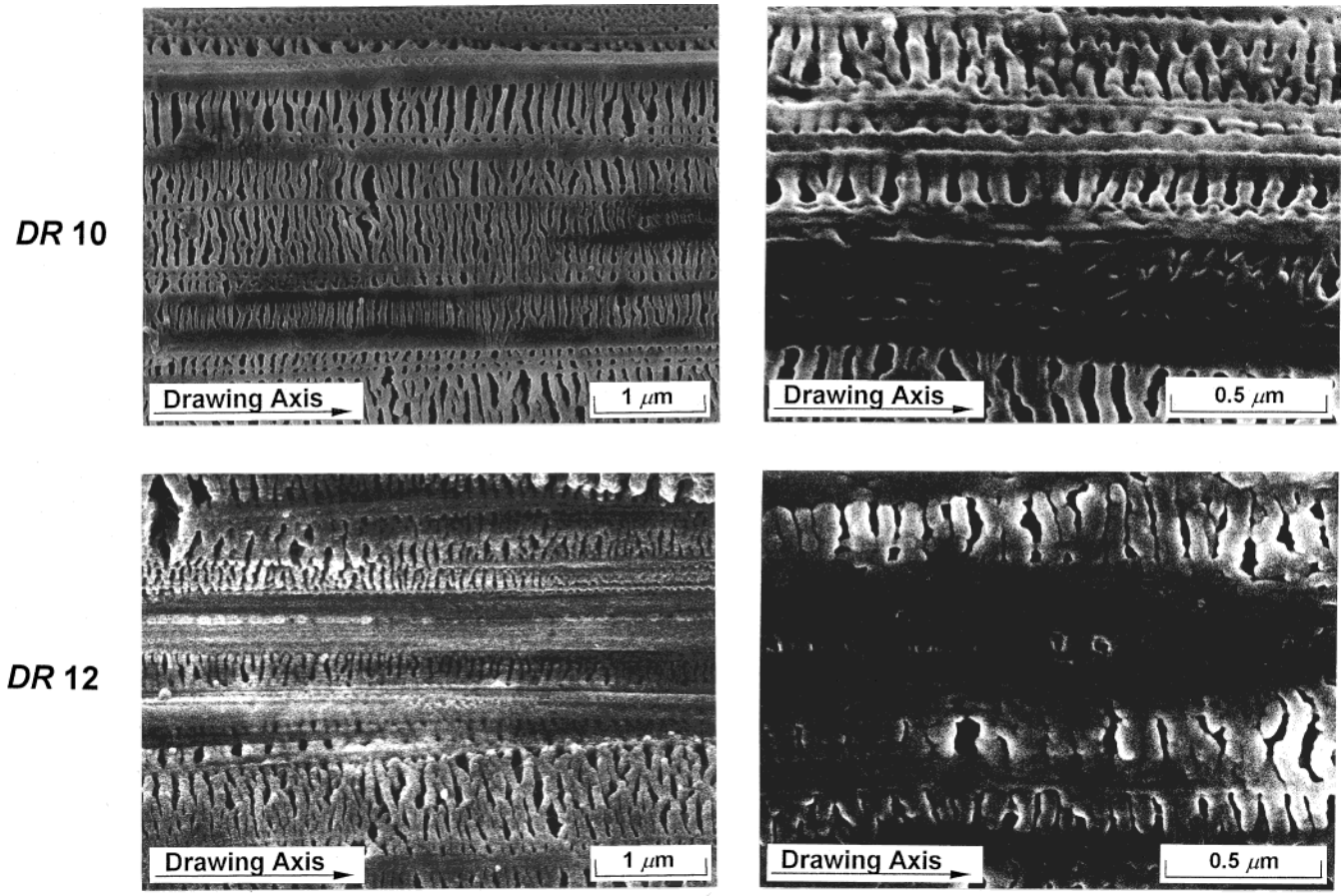

Figure 3. SEM images of MGC films compression-molded at $T_p = 230$ °C for 5 min and drawn at $T_d = 150$ °C. The samples were etched by fuming nitric acid at 60 °C for 48 h. The sets of the left and right photographs correspond to low- and high-magnification images, respectively.

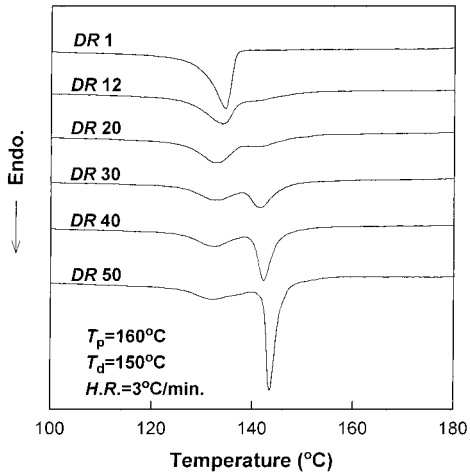

Figure 4. DSC melting thermograms for a DR series prepared at $T_d = 150$ °C from an MGC film prior-molded at $T_p = 160$ °C for 5 min.

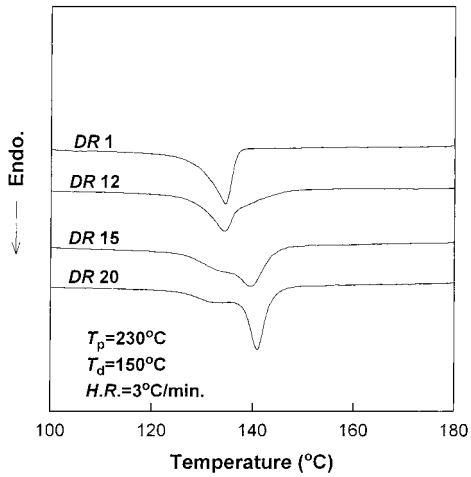

Figure 5. Changes in DSC melting thermograms on melt drawing at $T_d = 150$ °C of an MGC film prior-molded at $T_p = 230$ °C for 5 min.

exist within the "shish" components, may have a minor contribution to the overall endotherm compared to the heat of melting for crystals.

It has been shown by Keller et al.[36] that the DSC thermogram of a high-molecular-weight polyethylene fiber with "shish kebab" morphology, prepared by melt extrusion, exhibited a melting peak at ~130 °C and one or more peaks above 140 °C depending on the measurement condition. The lower peak was not affected by the measurement condition. However, the shape, size, and position of the higher melting peaks were sensitive to the constraints imposed on the sample in the course of measurement and could be altered by changing the constraints. Nevertheless, the low-temperature peak at 130 °C and the higher-temperature peaks at ~140 °C and above were ascribed to the melting of chain-folded lamellae and highly chain-extended structures, respectively.[36] As will be shown later, our samples also showed a broad peak at 134 °C and two more peaks above 150 °C, when measured under a constraint (Figure 9b). Thus, in our DSC measurements, special care was taken to avoid any external constraint on the sample. For this

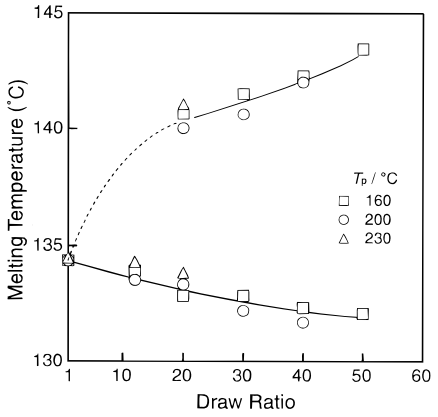

Figure 6. Peak melting temperatures as a function of DR for tensile drawing at $T_d = 150$ °C of the MGC series prepared at different T_p's. The melting time t_a was 5 min.

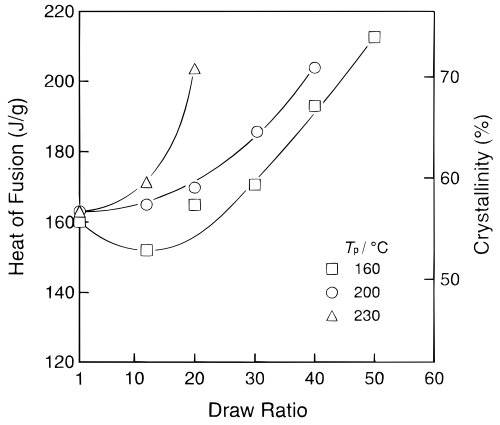

Figure 7. Total heat of fusion and crystallinity from DSC double melting peaks as a function of DR for the T_p series drawn at $T_d = 150$ °C.

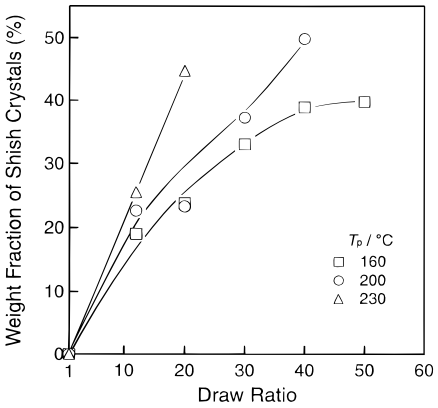

Figure 8. Fraction of "shish" crystals determined from the heat of fusion of the higher melting peak as a function of DR for tensile drawing at $T_d = 150$ °C of the MGC series prepared at the indicated temperatures (T_p in °C).

purpose, a small amount of silicone oil was placed between the sample and the bottom of the DSC sample pan, and the DSC scan was made without tightly cramping the pan. Thus, the shape, size, and position of the melting endotherm were highly reproducible. Therefore, the lower melting peak at 134 °C and the higher one around 140 °C were ascribed to the melting of the "kebob" and the "shish" components, respectively. Consistent with the SEM observations, these DSC results also indicate that the formation of "shish" crystals proceeded more rapidly for the former than for the latter, reflecting the significant effect of prior T_p on the property of molten UHMWPE.

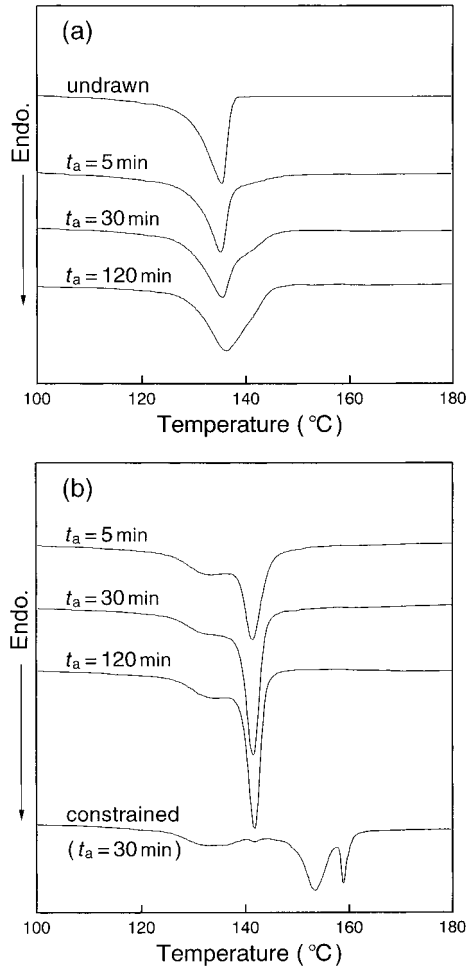

Figure 9. DSC thermograms for the samples of a DR of 12 (a) and 25 (b) series prepared from an MGC film prior-melt annealed at 200 °C for different times (t_a's). The thermogram of an undrawn MGC sample is also included in (a) for comparison. The effect of external constraints on the melting thermogram is illustrated with a sample of a DR of 25 prepared from the MGC film with $t_a = 30$ min (b).

Figure 6 shows the changes in the DSC double-melting-peak temperatures ($T_{m,peak}$) with DR for the different T_p series. At lower DR below 20, the $T_{m,peak}$ of the higher-temperature endotherm could not be determined because it appeared as a high-temperature shoulder of the lower melting peak. The $T_{m,peak}$'s of the double peaks at a given DR were not affected by the T_p and unique functions of DR, independent of the prior T_p. The higher $T_{m,peak}$ due to melting of the "shish" component[36] increased with DR from 140 °C around a DR of 20 to 143 °C at a DR of 50, near the DR_{max} of 60. The highest $T_{m,peak}$ of 143 °C was markedly higher than the $T_{m,peak}$ of the initial MGC films (~134 °C), crystallized by slowly cooling from the melt. Nevertheless, this value is significantly lower than the $T_{m,peak}$ of 146 °C observed on a superdrawn SGC mat of UHMWPE showing a tensile modulus of ~230 GPa, which is comparable to the X-ray crystal modulus of polyethylene.[4] These facts suggest that although the "shish" component consists of highly chain-extended crystals, the longitudinal crystallite sizes are limited probably due to the residual entanglements trapped within the "shish" component. Such a structure of the "shish"

component, in which "deep" entanglements are trapped, is similar to the morphological model proposed by Flory and Yoon[37] for the melt crystallization of polymers, where preexisting entanglements are concentrated in the noncrystalline regions. In contrast, the lower peak around 134 °C became slightly lower with DR, probably due to the formation of "kebob" crystals with lower-molecular-weight fractions with increasing DR during cooling of the drawn sample from the T_d (150 °C).

The actual T_m may increase with increasing the degree of segmental orientation in the melt due to a decrease in the entropy of the melt. Thus, the strain-induced crystallization above the static T_m is ascribed to the chain orientation in the melt, induced by the elongation of segments between entanglements during drawing. Further, the "deep" entanglements may effectively transmit the applied stress inducing segmental orientation, and such oriented segments may crystallize at an early stage of draw, as previously suggested on the basis of the stress/strain curves.[27]

Figure 7 shows characteristic features for the development of crystallinity as a function of DR, as determined from the total heat of fusion for the DSC double melting peaks. At a lower DR region ≤12, the crystallinity slightly decreased or increased depending on the T_p. At higher DR, the crystallinity increased rapidly and steadily with DR for every T_p series. Further, it was noted that the crystallinity increased more rapidly with DR for the MGC films prepared at higher T_p's. Although there were small differences in the crystallinity values determined from the heat of fusion and the density for a given sample, the effect of T_p on the crystallinity development determined by these DSC measurements is consistent with that estimated from the density data combined with the DR_{max} in Table 1, as discussed above.

The development of "shish" crystals with increasing DR was evaluated by the heat of fusion for the higher-temperature peak, as shown in Figure 8. The fractions of the "shish" component estimated from the DSC data are consistent with those observed in the SEM micrographs (Figures 1 and 2). For every T_p series, the "shish" crystals increased rapidly with DR. Further, it was noted that the amount of the "shish" component at a given DR increased for the drawing of MGC films prepared at higher T_p's. However, as the DR_{max} decreased with increasing T_p, the fraction reached comparable values of 40−50% around DR_{max} for all the T_p series. The fact that the "shish" component grew more rapidly for the sample with a higher T_p than for the one with a lower T_p suggests that, due to their difficulty of disentanglement, the "deeper" entanglements formed at a higher T_p transmitted the applied stress during drawing from the melt more effectively than "less deep" ones formed at a prior lower T_p.

As discussed, the T_p has an important effect on the formation of the "shish" component. In a previous paper,[27] it was found that the t_a also had a marked effect on the stress/strain curves for the melt-drawing of MGC films. The stress for an MGC sample prior-treated at 200 °C for a longer t_a increased more rapidly with strain than for one with shorter t_a. The result suggested that the number of "deep" entanglements, which might effectively transmit the draw stress within a molten sample, increased with increasing t_a. Thus, the effect of t_a on the morphology development during drawing was also evaluated by the DSC melting behavior of drawn products prepared from a series of MGC samples melt annealed at 200 °C for different t_a.

Parts a and b of Figure 9 show DSC melting thermograms for the samples of DR = 12 and 25, respectively, prepared from the MGC films prior-melt annealed at 200 °C for different t_a's of 5−120 min. A thermogram for an undrawn film with t_a = 5 min was also included in Figure 9a for comparison. Independent of the t_a, the DSC melting characteristics for undrawn samples were identical. The MGC sample showed a single melting peak at 134 °C. Upon drawing to a DR of 12, the products exhibited a shoulder at a higher-temperature side of the initial melting peak at 134 °C. Such a shoulder was more prominent for the drawing of a sample with a longer t_a than for one with a shorter t_a. As shown in Figure 9b, at a higher DR of 25 which corresponds to the DR_{max} for the MGC film with T_p = 200 °C and t_a = 120 min, each thermogram showed a clear melting peak around 141 °C and a broad one at 134 °C. However, when the measurements were made on these samples kept under constraints, the melting curves exhibited a broad peak at 134 °C and two more peaks at around 153 and 159 °C (Figure 9b), as reported.[35,36] These observations reveal the growth of a significant amount of the "shish" component at a DR of 25. Further, at a given DR, both the relative area of the higher melting peak and the crystallinity calculated from the total heat of fusion for the double peaks were greater for a sample with a longer t_a than for one with a shorter t_a. These DSC results confirm our previous conclusion[27] that increasing of t_a has a comparable effect to increasing T_p on the drawing characteristics and morphology development.

WAXD and SAXS Measurements. The morphology development was also examined by WAXD and SAXS. Figure 10 shows WAXD and SAXS photographs recorded at RT for an undrawn MGC film prior-melt annealed at T_p = 160 °C for 5 min and its DR series prepared at T_d = 150 °C. The WAXD pattern of the initial film exhibited uniform rings, indicating that the chains were randomly oriented within the sample. Upon drawing, the WAXD intensity distribution along the azimuthal direction became narrower and concentrated on the equator for each reflection, indicating that the chains were orientated with increasing DR. It is noted that at a DR of 12 the (200) reflection has two intensity maxima, one on the equator and the other one at an angle of 40° from the equator, whereas the (020) reflection appeared as a well-defined single arc on the equator. This indicates that the *a*-axis preferentially orients both perpendicularly to the fiber axis and at an angle of 50° from this axis. In contrast, the *b*-axis preferentially orients perpendicularly to the fiber axis. Such a characteristic chain orientation was previously reported for the melt-spinning of high-density polyethylene[38] and is significantly different from that observed in the crystalline-state deformation of spherillitic samples[39] and SGC mats of polyethylene.[3,4] At a DR > 30, each of the (*hk*0) reflections consisted of a strong circular spot on the equator overlapped with a weak and broad arc centered on the equator. This indicates that most of the crystalline chains are highly oriented along the fiber direction with a small amount of poorly oriented crystals. A closer inspection of the WAXD patterns for highly drawn samples (DR of 30 and 50) shows the appearance of a weak streak on the equator. Such a streak disappeared upon annealing the samples

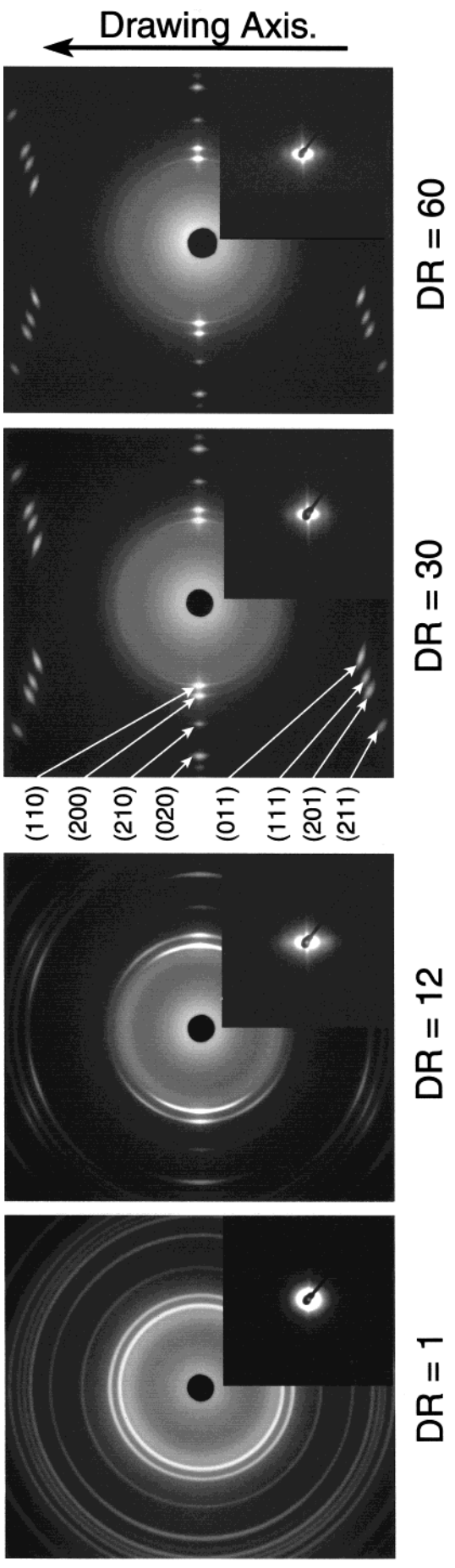

Figure 10. WAXD and SAXS (bottom right) patterns for a draw ratio series prepared from the MGC film prior-melted at 160 °C for 5 min.

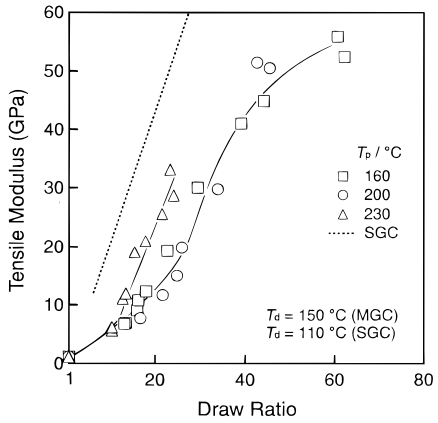

Figure 11. Tensile modulus vs DR for melt drawing of the MGC series compression-molded at the indicated T_p's for 5 min. Draw was made at T_d = 150 °C. The data for drawing of an SGC mat in the crystalline state at T_d = 110 °C are also included for comparison (dotted line).

at 120 °C, suggesting the existence of a small amount of thermally unstable crystallites with small lateral dimensions within the as-drawn products.

The SAXS patterns, inserted at the bottom of the WAXD photographs in Figure 10, also show the development of an oriented structure upon drawing. The MGC film showed SAXS around the direct beam, but no scattering maximum was distinguishable. Upon drawing to a DR > 12, a strong spotty scattering appeared on the meridian near the direct beam, suggesting the existence of distinct lamellar crystals oriented perpendicularly to the fiber axis. At a higher angle of the strong scattering, a weak scattering was observed, which could be assigned to the second-order scattering. Because the intensity maximum of the first-order scattering could not be distinguished due to the interference with the beam stopper, a long period was estimated from the second-order scattering maximum. The value of long period thus obtained was not significantly affected by the DR and 30−35 nm for the DR range of 12−60.

The crystalline core thickness, calculated from the SEM micrographs in Figures 1 and 2, was in the range 30−50 nm depending on the lamellae. Since the SAXS long period corresponds to the sum of the crystal core and the amorphous layer thickness of the lamellae, it would be expected to be longer than the one observed by SEM. The reason for this discrepancy is not clear. However, it is possible that the thinner lamellae were selectively etched and removed by fuming nitric acid treatment and only thicker lamellae survived after etching. Such a possibility is supported by the presence of many voids that are markedly larger than the crystal thickness, as seen in Figures 1 and 2.

Tensile Properties on Draw. The development of tensile properties upon the draw from melt was determined for the different T_p series. Figures 11 and 12 respectively show the tensile moduli and strengths as a function of DR for the drawing from melts of MGC films prepared at different T_p's. The draw was made at an optimum T_d of 150 °C and at constant cross-head speeds giving an initial strain rate of 5 min^{-1}. For comparison, the data obtained for solid-state drawing of a less entangled SGC mat (T_d = 110 °C) are also included. For each sample, both the tensile modulus and strength steadily increased with DR. As discussed above, the developments of both the crystallinity and the "shish" component were more rapid for the melt

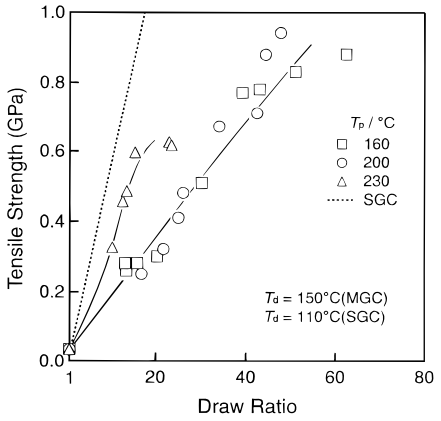

Figure 12. Tensile strength vs DR for melt drawing of MGC series compression-molded at the indicated T_p's for 5 min. The data for drawing of SGC mats are also shown by the dotted line for comparison.

drawing of the MGC films prior-compression-molded at higher T_p's (Figure 9). This likely suggests that the tensile properties may increase more rapidly for the drawing of MGC films molded at higher T_p's as well. In contrast to such an expectation, the slopes of these plots of tensile modulus and strength vs DR are comparable for all the samples prior-melted at $T_p = 160-200$ °C. This may be due to the fact that the differences in the amounts of "shish" component in these samples are minor and that the tensile properties not only depend on the amount of the chain-extended "shish" component but also the "kebob" lamellae significantly contribute to them through the intermeshing like a zip.[26,36] However, the slopes for drawing of the film prior-compressed at the highest T_p of 230 °C are larger than others, showing that the efficiency of draw, as evaluated from these tensile properties vs DR, is higher for this film than for others prior-molded at lower T_d's. This is consistent with the markedly more rapid increase in the "shish" component for drawing of this sample than for others with lower T_p's. These trends suggest that there are entanglements of different depths, depending on the prior T_p and the draw rate and temperature.[27] The "deep" entanglements formed at the highest T_p of 230 °C resulted upon draw in a rapid chain extension and orientation. Thus, high tensile properties were obtained at the same DR, compared to those of the samples drawn from the films prepared at lower T_p's.

On melt drawing of these films, the tensile properties increased with DR more gently than those for solid-state drawing of SGC mats.[4] These differences in their resultant tensile properties could be attributed to the differences in their morphologies. The sample drawn from SGC mats in the solid state has a higher crystallinity of ~90% at a DR around 60, whereas that of the melt-drawn MGC film was ~70% as shown in Table 1. Further, most of the crystals in the drawn SGC mats are highly extended along the draw direction, but the latter has a "shish kebab" structure at the same DR. As shown in Figure 8, the fraction of the highly oriented "shish" component reached a maximum of ~40% for the MGC films drawn from the melts. In fact, at the same DR of 60, the modulus of the drawn SGC mats approached higher values around 150−170 GPa, whereas that of the melt-drawn films exhibited a much lower value near 50−60 GPa, corresponding to 35% of the former.

In the melt drawing of UHMWPE, the maximum tensile modulus of 50−60 GPa and strength of 0.90−0.95 GPa were achieved at DR_{max} of ~60 by optimizing the drawing variables, including T_p, T_d, and draw rate. These values are significantly higher than those previously reported by Kaito et al.[24] for melt drawing of a molecular weight series of UHMWPEs. However, they are comparable to those reported by Bashir and Keller[26] for melt drawing of PE samples with a range of molecular weights. DR_{max} of the MGC films prepared at the highest T_p = 230 °C was limited up to 23, with the resultant tensile modulus and strength of 30 and 0.6 GPa, respectively, significantly lower than those obtained for drawing from the MGC films molded at lower prior T_p's.

Conclusions

In this work, MGC films prepared by compression-molding of UHMWPE reactor powder at different T_d's were uniaxially drawn at an optimum T_d of 150 °C in an air oven, about 15 °C above their melting temperatures. The films could be effectively drawn from a molten state up to DR_{max} of ~60 under controlled conditions, and the maximum tensile modulus and strength achieved up to 50−60 and 0.90−0.95 GPa, respectively. The drawability of the MGC film and the development of the oriented structure and tensile properties were found to be strongly affected by the prior-melt temperature on molding. SEM observations of etched samples showed that a "shish kebab" structure was developed during drawing from the melts. Correspondingly, DSC double melting endotherms were observed. The higher and lower melting peaks were attributed to the melting of chain-extended "shish" and chain-folded "kebob" crystals, respectively. The "shish" component increased with DR for all the series of films prepared at different prior-melt temperatures. The crystallization rate into such chain-extended "shish" crystals was higher for the drawing from the films prepared at a higher prior-melt temperature and/or for a longer melt-treatment time, probably due to the "deeper" level of entanglement formation associated with large-scale segmental diffusion in the prior-melts. The tensile properties of melt-drawn samples also reflect a similar effect of entanglement characteristics as a function of the prior-melt temperature.

References and Notes

(1) Smith, P.; Lemstra, P. J. *Colloid Polym. Sci.* **1980**, *258*, 891.
(2) Matuo, M.; Sawatari, C. *Macromolecules* **1986**, *19*, 2036.
(3) Furuhata, K.; Yokokawa, T.; Miyasaka, K. *J. Polym. Sci., Polym. Phys. Ed.* **1984**, *22*, 1330.
(4) Kanamoto, T.; Tsuruta, A.; Tanaka, K.; Takeda, M.; Porter, R. S. *Macromolecules* **1988**, *21*, 47.
(5) Kanamoto, T.; Tsuruta, A.; Tanaka, K.; Takeda, M. *Polym. J.* **1984**, *16*, 87.
(6) Peguy, A.; John Manley, R. St. *Polym. Commun.* **1984**, *25*, 39.
(7) Kanamoto, T.; Ohtsu, O. *Polym. J.* **1988**, *20*, 179.
(8) Huang, B.; Ito, M.; Kanamoto, T. *Polymer* **1994**, *35*, 1210.
(9) Yamane, A.; Sawai, D.; Kanamoto, T.; Ito, M.; Porter, R. S. *Macromolecules* **1997**, *30*, 4170.
(10) Sawai, D.; Yamane, A.; Kanamoto, T.; Ito, M.; Porter, R. S. *J. Polym. Sci., Polym. Phys. Ed.* **1998**, *36*, 629.
(11) Smith, P.; Lemstra, P. J.; Booij, H. C. *J. Polym. Sci., Polym. Phys. Ed.* **1981**, *19*, 877.
(12) Zachariades, A. E.; Watts, M. P. C.; Kanamoto, T.; Porter, R. S. *J. Polym. Sci. Lett. Ed.* **1978**, *17*, 487.
(13) Pawlikowski, G. T.; Mitchell, D. J.; Porter, R. S. *J. Polym. Sci., Polym. Phys. Ed.* **1988**, *26*, 1865.

(14) Kanamoto, T.; Ohama, T.; Tanaka, K.; Takeda, M.; Porter, R. S. *Polymer* **1987**, *28*, 1617.
(15) Griswold, P. D.; Zachariades, A. E.; Porter, R. S. *Polym. Eng. Sci.* **1978**, *18*, 861.
(16) Smith, P.; Chanzy, H. D.; Rotzinger, B. P. *Polym. Commun.* **1985**, *26*, 258.
(17) Smith, P.; Chanzy, H. D.; Rotzinger, B. P. *J. Mater. Sci.* **1987**, *22*, 523.
(18) Wang, L. H.; Ottani, S.; Porter, R. S. *Polymer* **1991**, *32*, 1776.
(19) Okuyama, H.; Kanamoto, T.; Porter, R. S. *J. Mater. Sci.* **1994**, *29*, 6485.
(20) Kameda, T.; Yamane, A.; Kanamoto, T.; Ito, M.; Porter, R. S. *Vysokomol. Soed., Ser. A* **1996**, *38*, 1152.
(21) Lemstra, P. J.; Van Aerle, N. A. J. M.; Bastiaannsen, C. W. M. *Polym. J.* **1987**, *19*, 85.
(22) Rahl, F. J.; Evanco, M. A.; Fredericks, R. J.; Reimschuessel, A. C. *J. Polym. Sci., Part A-2* **1972**, *10*, 1337.
(23) Yamaguchi, S. *Koubunshi Ronbunshuu* **1982**, *39*, 493.
(24) Kaito, A.; Nakayama, K.; Kanetuna, H. *Polym. J.* **1982**, *14*, 757.
(25) Van Aerle, N. A. J. M.; Lemstra, P. J. *Makromol. Chem.* **1988**, *189*, 1253.
(26) Bashir, Z.; Keller, A. *Colloid Polym. Sci.* **1989**, *267*, 116.
(27) Uehara, H.; Nakae, M.; Kanamoto, T.; Zachariades, A. E.; Porter, R. S. *Macromolecules* **1999**, *32*, 2761.
(28) Wunderlich, B. *Macromolecular Physics*; Academic Press: New York, 1973; Vol. 1.
(29) Uehara, H.; Nakae, M.; Kanamoto, T.; Ohtsu, O.; Sano; A.; Matsuura, K. *Polymer* **1998**, *39*, 6127.
(30) Zachariades, A. E. *Polym. Eng. Sci.* **1985**, *25*, 747.
(31) Xue, Y. Q.; Tervoot, T. A.; Lemstra, P. J. *Macromolecules* **1998**, *31*, 3075.
(32) Barham, P. J.; Sadler, D. M. *Polymer* **1991**, *32*, 393.
(33) Souffache, E. R.; Rault, J. *Macromolecules* **1984**, *17*, 337.
(34) Millaud, B.; Rault, J. *Macromolecules* **1984**, *17*, 340.
(35) Pennings, A. J. *J. Polym. Sci., Polym. Phys. Ed.* **1977**, *59*, 55.
(36) Bashir, Z.; Odell, J. A.; Keller, A. *J. Mater. Sci.* **1986**, *21*, 3993.
(37) Flory, P. J.; Yoon, D. Y. *Nature* **1978**, *272*, 226.
(38) Katayama, K.; Amano, T.; Nakayama, K. *Kolloid Z. Z. Polym.* **1968**, *226*, 125.
(39) Kasai, N.; Kakudo, M. *J. Polym. Sci., Part A* **1964**, *2*, 1955.

MA991330A